Inorganic Chemistry

Article

pubs.acs.org/IC

Preparation and Dehydrogenation Properties of Lithium Hydrazidobis(borane) ($LiNH(BH_3)NH_2BH_3$)

He Fu, Junzhi Yang, Xiaojuan Wang, Gongbiao Xin, Jie Zheng, and Xingguo Li*

College of Chemistry and Molecular Engineering, Peking University, Beijing 100871, P. R. China

Supporting Information

ABSTRACT: $LiNH(BH_3)NH_2BH_3$, the first example of metal-substituted hydrazine bisborane (HBB), is synthesized via the reaction between HBB and *n*-butyllithium in ether solution. ^{11}B NMR and Fourier transform infrared spectroscopy indicate a new structure, in which one of the N−H bonds is replaced by a N−Li bond. The X-ray diffraction pattern of the product also indicates the formation of a new crystal structure. This compound releases hydrogen at 126 and 170 °C with satisfactory purity and exhibits superior hydrogen storage properties compared with HBB. Differential scanning calorimetry measurement suggests the dehydrogenation reaction of this compound is less exothermic than that of HBB.

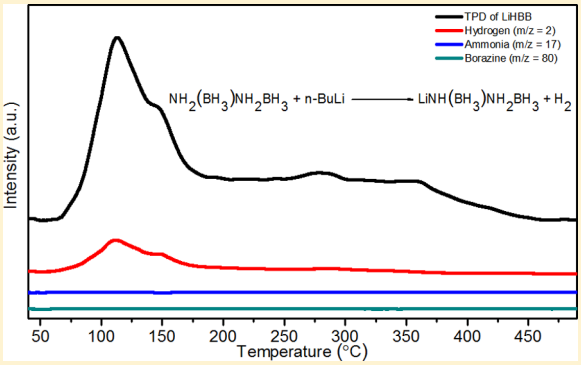

INTRODUCTION

Development of efficient and economic hydrogen storage materials is one of the most crucial steps for the utilization of hydrogen energy. Researchers have long been seeking for a proper hydrogen storage material with high gravimetric and volumetric capacity, moderate (de)hydrogenation conditions, and favorable reversibility.[1] Chemical hydrides based on the B−N Lewis pairs (e.g., ammonia borane (AB)) are considered to be one of the most promising candidates.[2] Although these materials can release hydrogen at low temperature, they are hampered by emission of byproducts and poor reversibility. Sutton et al. establishes a method to realize regeneration of AB from polyborazylene (PB), the main component in the spent fuel, to recover AB.[3] This finding stimulated further exploration of the B−N−H system with high H capacity, good dehydrogenation kinetics, and possible reversibility.

In addition to the well-studied AB system, it is also interesting to study the hydrogen storage properties of the more complicated B−N compounds. Hydrazine borane (HB) was investigated for its hydrogen storage properties in both hydrolysis and pyrolysis. When catalyzed by Rh[4] or Ni−Pt nanoparticles,[5] HB reacts with water to produce H_2, N_2, and NH_3. HB can also dehydrogenate in tetrahydrofuran (THF) with group 4 metallocene alkyne complexes as catalyst.[6] During thermal decomposition, HB dehydrogenates at low temperature but is accompanied by toxic N_2H_4 and NH_3.[7] The thermal decomposition of a similar compound with more complicated structure, hydrazine bisborane (HBB), is also investigated.[8] Research shows that the decomposition of HBB takes place at mild temperature, accompanied by a trace amount of ammonia in the second step. However, HBB is explosive upon heating to 160 °C at a rate of 10 K/min.[9] This could cause a safety concern for on-board hydrogen storage applications.

Recently, lithium hydrazidoborane (LiHB) and its hydrazine borane adducts (LiHB·2HB) were synthesized and show minimized toxic gas release, indicating that the Li substitution might lead to improved hydrogen-release properties.[10] Na substitution of HB is also found to have similar effects.[11] This is in agreement with the well-known metal substitution effect in ammonia borane.[12] Therefore, it is highly interesting to study whether a similar strategy can also be applied in B−N compounds with a more complicated structure like HBB.

Metal substitution of the B−N compounds is commonly achieved by ball milling of the metal hydride with the corresponding B−N compounds.[13] The driving force is the recombination of the hydridic $H^{\delta-}$ in the metal hydride with the protonic $H^{\delta+}$ binding to the N atom. However, this approach is not applicable to HBB, as HBB is shock-sensitive and explodes even under mild ball-milling conditions. A completely different reaction strategy, therefore, is required to achieve metal substitution on HBB.

The key step for the metal substitution is deprotonation of the amino group in B−N compounds. A strong Lewis base, therefore, is favorable for the reaction. In fact, the metal hydride approach is based on the similar idea. Several kinds of strong Lewis base have been reported in the deprotonation reaction of ammonia borane.[14] Here we demonstrate that by using *n*-butyllithium (*n*-BuLi), lithium substitution on HBB can be efficiently achieved in ether solution. The reaction proceeds according to the following equation (eq 1):

Received: March 24, 2014
Published: June 27, 2014

dx.doi.org/10.1021/ic500679b | Inorg. Chem. 2014, 53, 7334−7339

$$NH_2(BH_3)NH_2BH_3 + n\text{-BuLi} \rightarrow LiNH(BH_3)NH_2BH_3 + n\text{-}C_4H_{10} \quad (1)$$

EXPERIMENTAL SECTION

Materials. The starting materials, namely, hydrazine sulfate (98%) and sodium borohydride (95%), were purchased from Sinopharm Chemical Reagents Co., Ltd. and were used as received, without further purification. The *n*-BuLi (2.4 mol/L in hexanes) was purchased from J&K Chemical. Diethyl ether (Et_2O) or THF was treated in a 500 mL round-bottom flask with sodium granules for 12 h with benzophenone as an indicator to remove water and peroxides. After the solution turned blue, the solvent was distilled and collected in a 500 mL Schlenk flask. All the materials mentioned above were stored in an argon-filled glovebox.

Nuclear Magnetic Resonance (NMR). ^{11}B NMR spectra were collected for liquid samples on a Bruker AVANCE III 500 MHz spectrometer. ^{11}B MAS NMR experiments were performed on a Bruker AVANCE III 400 MHz WB Solid-State NMR spectrometer. The sample was loaded into a 4 mm ZrO_2 sample tube in an Ar-filled glovebox. The spectra were collected at a spin rate of 12 kHz. A one-pulse excitation program was employed. All the NMR data were referenced to $BF_3{\cdot}Et_2O$ (at 0 ppm) as an external standard material.

Temperature-Programmed Desorption/Mass Spectroscopy. TPD/MS experiments were performed on a Quantachrome Autosorb iQ automatic gas sorption analyzer. The sample (20 mg) was capped by quartz wool and was loaded in a U-shaped sample cell with a quartz filler rod. The sample was heated in a high-purity argon (99.999%) flow of 50 mL/min. The gaseous product was first allowed to flow through a thermal conductivity detector (TCD) to determine the total amount of gaseous product. The gas composition was further analyzed by a Pfeiffer PrismaPlus Mass Spectrometer/Residual Gas Analyzer (MS/RGA). Two needle valves, namely, a vent sampling valve and a mass spectrometer input valve, were adjusted to introduce proper amount of gas into the mass spectrometer. The scan mode (from m/z = 0 to m/z = 200 amu) was employed at a scan rate of approximately 2 cycles/min to obtain the composition of the gaseous products. The multiple ion detection (MID) mode was used to analyze the temporal variation of specific products. The m/z value for the detection channels was determined according to a built-in database of the instrument. Temperature was simultaneously measured by a thermocouple installed close to the sample cell. The heating rate was 5 K/min for LiHBB samples and 2 K/min for HBB samples. A gross leak test was performed before each experiment.

X-ray Photoelectron Spectroscopy. The X-ray photoelectron spectroscopy (XPS) analysis was performed on an AXIS-Ultra spectrometer (Kratos Analytical) using monochromatic Al Kα radiation (225 W, 15 mA, 15 kV). The step of binding energy was 0.1 eV. All the binding energies were referenced to C 1s at 284.6 eV.

Powder X-ray Diffraction. The crystal structure of reactants and products were characterized by X-ray diffraction (XRD, Rigaku D/max 200 diffractometer, Cu Kα) at a scan rate of 2°/min.

Fourier Transform Infrared Spectroscopy. The FT-IR spectra of LiHBB and HBB were collected on a Nicolet iN10 MX microscope FT-IR spectrometer in the range from 599 to 4000 cm^{-1}.

Differential Scanning Calorimetry. DSC measurement was performed on a Netzsch DSC 204 HP calorimeter. The sample (5.0 to 10.0 mg) was loaded in an aluminum crucible in an argon-filled glovebox. The crucible was covered by an aluminum lid with a pinhole on it allowing gaseous product to escape. The experiments were performed in an inert gas flow (high purity argon, 99.999%, 50 mL/min, 1.0 bar) with a heating rate of 2 K/min.

Hydrogen Desorption Measurement. The gravimetric hydrogen capacity of LiHBB and HBB samples were obtained using Hy-Energy PCT Pro-2000 instrument (Setaram Inc.). The sample (50 mg) was loaded in a stainless steel sample holder and sealed with a VCR connector. The chamber pressure and temperature were monitored by the instrument and were converted to the amount of hydrogen desorbed. The dehydrogenation was carried out through multiple temperature stages at 130, 150, 180, 210, and 350 °C, which were chosen according to the onset and peak temperature in TPD/MS results.

Preparation of Hydrazine Bisborane. Hydrazine sulfate (2.512 g, 18.9 mmol) and sodium borohydride (1.485g, 37.1 mmol) were gently milled in an agate mortar for 10 min in an argon-filled glovebox. The solid mixture was added to a 500 mL round-bottom flask and connected to the Schlenk line. Anhydrous THF was quickly introduced into the flask under stirring to yield a suspension. After stirring under argon atmosphere at 40 °C for 80 h, the suspension was filtered, and the supernatant was evacuated to get a white powder. The powder was held in vacuum for 24 h under stirring to remove the solvents to obtain HBB (0.810 g, yield 69.9%).

Preparation of Lithium Hydrazidobisborane. The preparation was carried out in an Ar-filled glovebox. HBB (0.120 g, 2.00 mmol) was dissolved in 300 mL of anhydrous diethyl ether in a 500 mL round-bottom flask under stirring. 0.8 mL of *n*-BuLi was diluted in 50 mL of anhydrous diethyl ether. Then the *n*-BuLi/ether solution was added dropwise into the flask over 20 min. Precipitation was observed immediately when the two solutions made contact. The mixture was stirred at room temperature for 4 h to complete the reaction. The precipitation was filtered to get a gray solid product. The product was dried under dynamic vacuum at room temperature overnight to get a white powder (0.069 g, 52.3%).

RESULTS AND DISCUSSION

The ^{11}B NMR spectra of LiHBB and pristine HBB are shown in Figure 1. The NMR spectrum of HBB exhibits a quartet

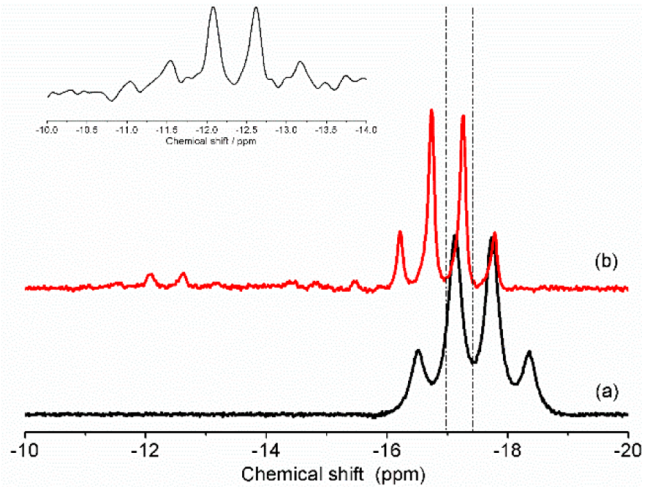

Figure 1. ^{11}B NMR spectra of (a) HBB and (b) LiHBB in diethyl ether solution. (inset) The details of spectrum (b) in the chemical shift range from −10 to −14 ppm. For spectrum in larger scale, see Supporting Information, Figure S1.

centered at −17.5 ppm, which can be assigned to the two identical BH_3 groups.[15] In the NMR spectrum of LiHBB, the quartet at −17.5 ppm disappears. Two sets of quartets at −16.9 ppm and −12.3 ppm are found in the spectrum, indicating that the two BH_3 groups are in different chemical environments. The quartet at −12.3 ppm can be attributed to the BH_3 group attached to the lithium-substituted nitrogen atom. The strong electron-withdrawing inductive (-I) effect of Li^+ lowers the electron density on the adjacent BH_3 group and causes a shift of the lower field. For the BH_3 group at the other end of the molecule, this inductive effect is weak due to the increased distance; thus, only a very slight shift to the lower field (−16.7 ppm) results in this case.

dx.doi.org/10.1021/ic500679b | Inorg. Chem. 2014, 53, 7334−7339

Figure 2 is the powder X-ray diffraction (PXRD) patterns of HBB and LiHBB. The PXRD pattern of HBB is in accordance

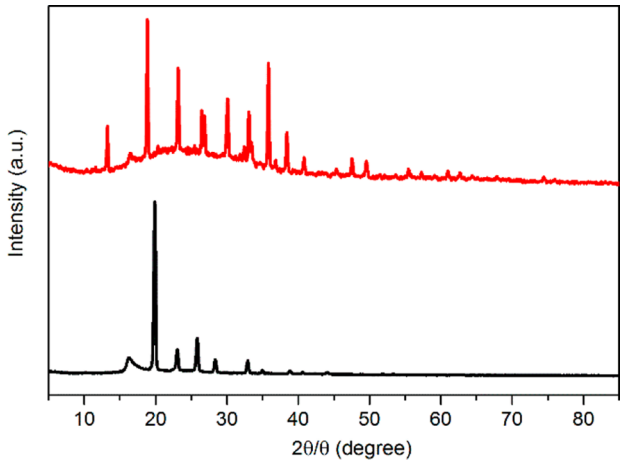

Figure 2. PXRD pattern of as-synthesized LiHBB (red) and HBB (black).

to the reported results.[8] The Li-substituted sample exhibits a distinct pattern corresponding to a new phase. All the diffraction peaks of HBB disappear after the reaction, indicating complete conversion of HBB.

Figure 3a shows the FT-IR spectra of HBB and LiHBB. In the low-frequency region (below 1600 cm^{-1}), the signals are mainly assigned to the stretching of the B−N and N−N bonds in the skeleton.[16] The shoulder peak at 1602 cm^{-1} may be assigned to B−H scissoring. In the midfrequency region from 2200 to 2600 cm^{-1}, the peaks are assigned to the B−H stretching modes (ν_{B-H} = 2287 and 2350 cm^{-1}).[17] In the frequency range above 3000 cm^{-1}, the signals are assigned to symmetric and asymmetric stretching of N−H bonds.[18] Although the spectra of HBB and LiHBB are quite similar, a few appreciable new features are observed for the N−H stretching modes. The weak peaks at 3336 cm^{-1} could be attributed to the stretching of the N−H bond adjacent to lithium, which occurs at a slightly higher frequency than that of the NH_2 group (3133 and 3226 cm^{-1}).[19] This frequency shift is attributed to the strengthening of N−H bonds when the other H atom is substituted by lithium. The strong inductive effect of lithium ion would attribute to the redistribution of the electron density between N and H atoms. The X-ray photoelectron spectroscopy (XPS) results (Figure 3b) show that the binding energies of N 1s electrons in both HBB and LiHBB samples are relatively low (398.0 eV in LiHBB and 399.1 eV in HBB). This indicates that N atoms in both compounds are in low oxidation state. The binding energy of N 1s electron in LiHBB is slightly lower than that in HBB. This observation is in accordance with the increase of electron density on the N atom due to the electron transfer from Li to N.[20]

The above structural characterization suggests that the new phase shows features corresponding to Li substitution of one H on the NH_2 group. It is the strong deprotonation ability of the strong Lewis base *n*-BuLi that contributes to the successful substitution. Similar attempts employing *n*-BuLi as a deprotonation reagent can also be found in the pioneering work by Fisher et al.,[21] who have synthesized a number of metal-substituted aminoborohydride derivatives by a similar method. A key advantage of this method over the widely used metal hydride-based approach[22] is that *n*-BuLi is soluble in diethyl ether, which allows more rapid reaction and easier product separation. This method can also be readily extended to the synthesis of the metal derivatives of more vulnerable B−N−H compounds.

The Li substitution dramatically influences the hydrogen storage properties of HBB. Temperature-programmed desorption and mass spectrometry (TPD/MS) curves of LiHBB and HBB (Figure 4) indicate that LiHBB performs better in both desorption temperature and gas purity. HBB dehydrogenates at 180, 212, and 252 °C. The last step of decomposition is accompanied by the emission of ammonia and borazine. LiHBB starts to decompose at around 100 °C and reaches the first gas release peak at 126 °C, while the second step occurs at 170 °C. At elevated temperature, the sample exhibits broad dehydrogenation peaks. It may be attributed to the gradual condensation of B−H and N−H accompanied by hydrogen evolution. During the whole decomposition process, no signals of gaseous byproducts are detected. This is a notable improvement compared to the pristine HBB.

To determine the gravimetric hydrogen capacity of LiHBB, we carried out a volumetric gas desorption experiment (Figure 5). We find that during the two dehydrogenation steps, the sample releases 4.4 and 3.8 wt % hydrogen at 150 and 350 °C,

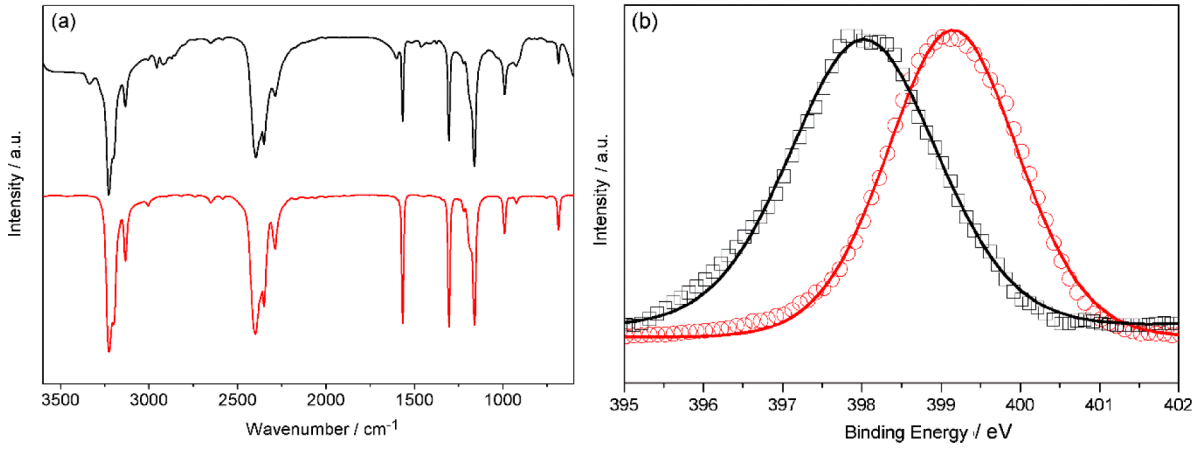

Figure 3. (a) FT-IR spectra of LiHBB (black) and HBB (red). (b) The N 1s XPS results of LiHBB (black) and HBB (red). The original data are shown in square and circle symbols while the fitted curves are shown in lines.

dx.doi.org/10.1021/ic500679b | *Inorg. Chem.* 2014, 53, 7334−7339

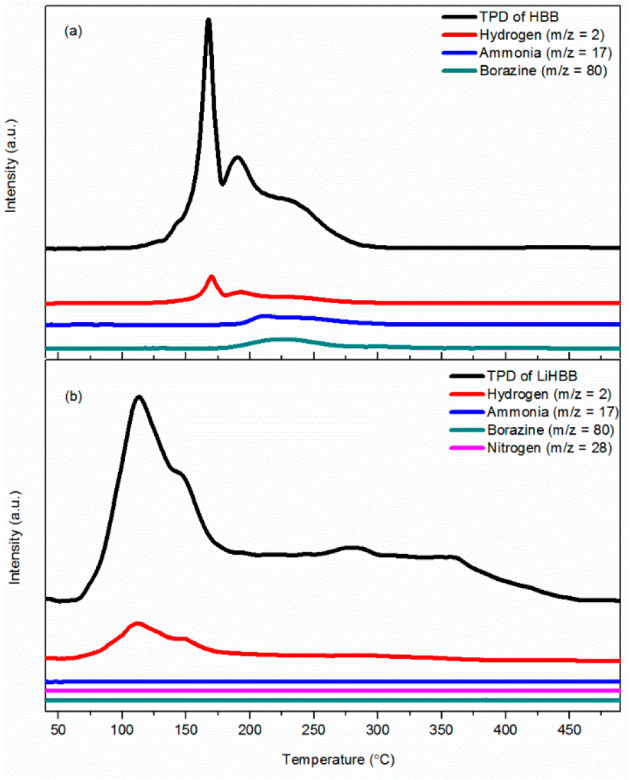

Figure 4. TPD/MS curves of (a) HBB and (b) LiHBB. The TPD signals from TCD device are demonstrated in black lines. MS signals from the release of hydrogen (m/z = 2), ammonia (m/z = 17), and borazine (m/z = 80) are demonstrated in red, blue, and green lines, respectively.

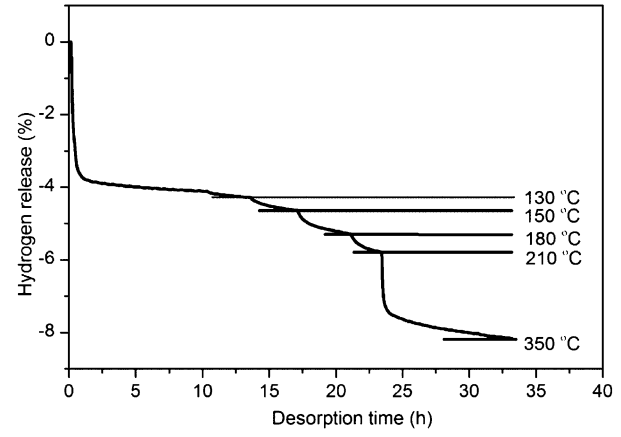

Figure 5. Volumetric hydrogen desorption curve for LiHBB samples at various temperatures.

respectively. On the basis of the amount of H_2 released, the two reactions can be described by eq 2 and eq 3:

$$\text{“}LiN_2B_2H_9\text{”} \rightarrow \text{“}LiN_2B_2H_6\text{”} + 1.5H_2 \quad (2)$$

$$\text{“}LiN_2B_2H_6\text{”} \rightarrow \text{“}LiN_2B_2H_{3.5}\text{”} + 1.25H_2 \quad (3)$$

DSC measurements were carried out to determine the thermodynamic properties of these two dehydrogenation processes (Figure 6). The decomposition of LiHBB is much less exothermic compared to that of the pristine HBB. The first decomposition step of LiHBB at 126 °C only shows a tiny exothermic peak corresponding to a very small enthalpy of 0.10

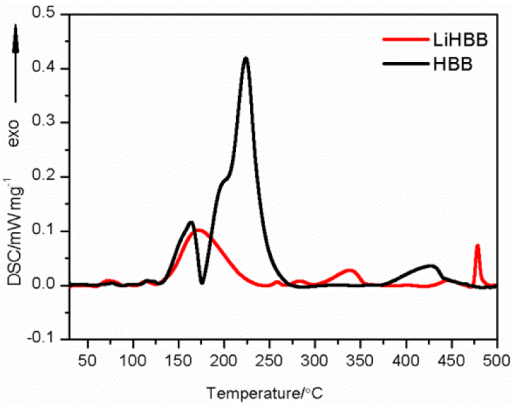

Figure 6. DSC measurements of LiHBB (red) and HBB (black) at a heating rate of 2 K/min under argon flow.

kJ/mol H_2. In the case of HBB, the enthalpy of the first decomposition step is 4.8 kJ/mol H_2. The exothermic dehydrogenation nature is a major thermodynamic obstacle for direct regeneration under hydrogen pressure.[23] The near zero dehydrogenation enthalpy of LiHBB makes it very likely to become thermodynamically favorable for hydrogenation by proper modification. Some endothermic examples have been found in the amidoborane ammoniates though the corresponding amidoboranes are exothermic upon dehydrogenation.[24] It suggests that the ammoniate of LiHBB may also lead to more favorable thermodynamic properties for on-board reversibility.

The small exothermic peaks above 250 °C reveal a complicated reaction pathway in the high-temperature region, which is also found in other B−N−H compounds.[25] It could be attributed to the formation of oligomers of B−N compounds and, at higher temperatures, polymeric chains and networks of azaborines. Figure 7 shows the ^{11}B magic-angle spinning

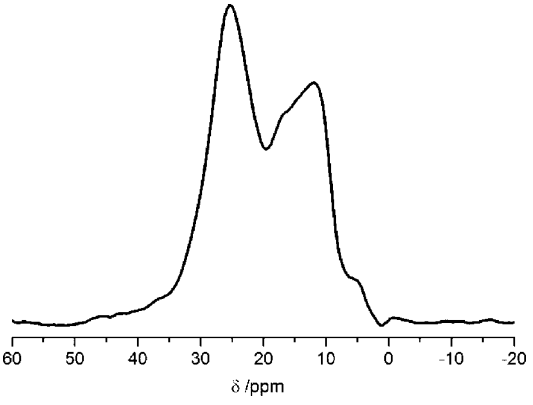

Figure 7. ^{11}B MAS NMR spectrum of the dehydrogenated residual of LiHBB.

(MAS) NMR spectrum of the decomposition product of LiHBB. The two strong resonance peaks at 16.9 and 25.4 ppm are assigned to the BN_3 and/or HBN_2 groups[26] that result from the intermolecular reactions. Compared to the reported results of spent fuel of ammonia borane and amidoboranes,[27] these resonance peaks shift to lower fields, which can be attributed to the -I effect of the Li^+ in the residual. The XRD pattern of this residue exhibits the presence of Li_3BO_3 and an unknown phase. No obvious peaks of BN are observed (see Supporting Information, Figure S2). The IR spectrum of the dehydro-

dx.doi.org/10.1021/ic500679b | Inorg. Chem. 2014, 53, 7334−7339

genated sample shows broadended N−H/B-H stretching bands, indicating the agglomeration of B−N−H species (Supporting Information, Figure S3).

The introduction of Li^+ alters the electronic structure of the molecule, which in turn significantly lowers the desorption temperature, suppresses the toxic gas release, and enhances the thermodynamic performance. These superior properties, together with the polymerization behavior found in Figure 7, indicate that the Li^+ cation may play an important role in both the formation of an intermediate and the condensation of B−N monomers and oligomers. Meanwhile, these advances in dehydrogenation properties are very similar to those reported in lithium amidoborane, which decomposes at 92 °C with no byproducts.[13a] The catalytic effect of Li^+ cations in lithium amidoborane has been widely investigated both experimentally and theoretically.[28] Zhang et al. propose that the formation of LiAB dimer $(LiAB)_2$ substantially reduces the energy barrier in the dehydrogenating reaction of LiAB.[28b] Kim et al. suggest that LiH forms through the hydride transfer from $NH_2BH_3^-$ to Li^+ and that LiH acts as a hydride donor in the hydrogen-evolving process of M−H···H−N dihydrogen bond.[28a] As to LiHBB, further experimental and theoretical investigation should be carried out to help us understand the different dehydrogenation behavior between HBB and LiHBB and reveal their actual dehydrogenation mechanism.

CONCLUSION

In conclusion, we synthesize the first metal-substituted derivative of HBB by reacting with a strong Lewis base, *n*-BuLi, in Et_2O solution. Compared to the widely adopted hydride approach for metal substitution, this method significantly enhances the reaction efficiency and facilitates the product separation. This compound starts to decompose at 100 °C and can release 8.2 wt % H_2 at 350 °C without detectable gaseous byproducts. The lithium substitution reduces the dehydrogenation enthalpy to near zero, which is promising candidate for on-board applications.

ASSOCIATED CONTENT

Supporting Information

Includes ^{11}B NMR of LiHBB, and XRD and IR of LiHBB residue. This material is available free of charge via the Internet at http://pubs.acs.org.

AUTHOR INFORMATION

Corresponding Author

*E-mail: xgli@pku.edu.cn. Fax: (+) 86-10-62765930.

Author Contributions

The manuscript was written through contributions of all authors. All authors have given approval to the final version of the manuscript.

Notes

The authors declare no competing financial interest.

ACKNOWLEDGMENTS

The authors acknowledge MOST of China (No. 2010CB631301 and 2012CBA01207) and NSFC (No. U1201241, 11375020, and 21321001).

REFERENCES

(1) (a) Graetz, J. *Chem. Soc. Rev.* **2009**, *38*, 73. (b) Hamilton, C. W.; Baker, R. T.; Staubitz, A.; Manners, I. *Chem. Soc. Rev.* **2009**, *38*, 279. (c) Orimo, S.-i.; Nakamori, Y.; Eliseo, J. R.; Zuettel, A.; Jensen, C. M. *Chem. Rev.* **2007**, *107*, 4111. (d) Woolf, H.; Brown, I.; Bowden, M. *Curr. Appl. Phys.* **2008**, *8*, 459.

(2) (a) Peng, B.; Chen, J. *Energy Environ. Sci.* **2008**, *1*, 479. (b) Hamilton, C. W.; Baker, R. T.; Staubitz, A.; Manners, I. *Chem. Soc. Rev.* **2009**, *38*, 279.

(3) Sutton, A. D.; Burrell, A. K.; Dixon, D. A.; Garner, E. B., III; Gordon, J. C.; Nakagawa, T.; Ott, K. C.; Robinson, P.; Vasiliu, M. *Science* **2011**, *331*, 1426.

(4) Karahan, S.; Zahmakiran, M.; Ozkar, S. *Int. J. Hydrogen Energy* **2011**, *36*, 4958.

(5) Hannauer, J.; Akdim, O.; Demirci, U. B.; Geantet, C.; Herrmann, J.-M.; Miele, P.; Xu, Q. *Energy Environ. Sci.* **2011**, *4*, 3355.

(6) Thomas, J.; Klahn, M.; Spannenberg, A.; Beweries, T. *Dalton Trans.* **2013**, *42*, 14668.

(7) (a) Huegle, T.; Kuehnel, M. F.; Lentz, D. *J. Am. Chem. Soc.* **2009**, *131*, 7444. (b) Moury, R.; Moussa, G.; Demirci, U. B.; Hannauer, J.; Bernard, S.; Petit, E.; van der Lee, A.; Miele, P. *Phys. Chem. Chem. Phys.* **2012**, *14*, 1768.

(8) Sun, W.; Gu, Q.; Guo, Y.; Guo, Z.; Liu, H.; Yu, X. *Int. J. Hydrogen Energy* **2011**, *36*, 13640.

(9) Gunderloy, F. C.; Spielvogel, B.; Parry, R. W. *Inorg. Synth.* **1967**, *9*, 13.

(10) Wu, H.; Zhou, W.; Pinkerton, F. E.; Udovic, T. J.; Yildirim, T.; Rush, J. J. *Energy Environ. Sci.* **2012**, *5*, 7531.

(11) Moury, R.; Demirci, U. B.; Ichikawa, T.; Filinchuk, Y.; Chiriac, R.; van der Lee, A.; Miele, P. *ChemSusChem* **2013**, *6*, 667.

(12) (a) Fijalkowski, K. J.; Jurczakowski, R.; Kozminski, W.; Grochala, W. *Phys. Chem. Chem. Phys.* **2012**, *14*, 5778. (b) Ramzan, M.; Silvearv, F.; Blomqvist, A.; Scheicher, R.; Lebègue, S.; Ahuja, R. *Phys. Rev. B* **2009**, *79*.

(13) (a) Xiong, Z.; Yong, C. K.; Wu, G.; Chen, P.; Shaw, W.; Karkamkar, A.; Autrey, T.; Jones, M. O.; Johnson, S. R.; Edwards, P. P.; David, W. I. F. *Nat. Mater.* **2007**, *7*, 138. (b) Zhang, Q.; Tang, C.; Fang, C.; Fang, F.; Sun, D.; Ouyang, L.; Zhu, M. *J. Phys. Chem. C* **2010**, *114*, 1709.

(14) (a) Myers, A. G.; Yang, H.; Kopecky, D. J. *Tetrahedron Lett.* **1996**, *37*, 3623. (b) Myers, A. G.; Yang, B. H.; Chen, H.; McKinstry, L.; Kopecky, D. J.; Gleason, J. L. *J. Am. Chem. Soc.* **1997**, 6496.

(15) Stowe, A. C.; Shaw, W. J.; Linehan, J. C.; Schmid, B.; Autrey, T. *Phys. Chem. Chem. Phys.* **2007**, *9*, 1831.

(16) Lee, S. M.; Kang, X. D.; Wang, P.; Cheng, H. M.; Lee, Y. H. *ChemPhysChem* **2009**, *10*, 1825.

(17) Renaudin, G.; Gomes, S.; Hagemann, H.; Keller, L.; Yvon, K. *J. Alloys Compd.* **2004**, *375*, 98.

(18) Kojima, Y.; Kawai, Y. *J. Alloys Compd.* **2005**, *395*, 236.

(19) Hu, J.; Fichtner, M.; Chen, P. *Chem. Mater.* **2008**, *20*, 7089.

(20) Li, L.; Yao, X.; Sun, C.; Du, A.; Cheng, L.; Zhu, Z.; Yu, C.; Zou, J.; Smith, S. C.; Wang, P.; Cheng, H.-M.; Frost, R. L.; Lu, G. Q. *Adv. Funct. Mater.* **2009**, *19*, 265.

(21) (a) Fisher, G. B.; Fuller, J. C.; Harrison, J.; Alvarez, S. G.; Burkhardt, E. R.; Goralski, C. T.; Singaram, B. *J. Org. Chem.* **1994**, *59*, 6378. (b) Fisher, G. B.; Harrison, J.; Fuller, J. C.; Goralski, C. T.; Singaram, B. *Tetrahedron Lett.* **1992**, *33*, 4533.

(22) (a) Xiong, Z.; Wu, G.; Chua, Y. S.; Hu, J.; He, T.; Xu, W.; Chen, P. *Energy Environ. Sci.* **2008**, *1*, 360. (b) Xiong, Z.; Chua, Y. S.; Wu, G.; Xu, W.; Chen, P.; Shaw, W.; Karkamkar, A.; Linehan, J.; Smurthwaite, T.; Autrey, T. *Chem. Commun.* **2008**, 5595.

(23) David, W. I. F. *Faraday Discuss.* **2011**, *151*, 399.

(24) Chua, Y. S.; Wu, G.; Xiong, Z.; He, T.; Chen, P. *Chem. Mater.* **2009**, *21*, 4899.

(25) (a) Pons, V.; Baker, R. T.; Szymczak, N. K.; Heldebrant, D. J.; Linehan, J. C.; Matus, M. H.; Grant, D. J.; Dixon, D. A. *Chem. Commun.* **2008**, 6597. (b) Bowden, M.; Autrey, T. *Curr. Opin. Solid State Mater. Sci.* **2011**, *15*, 73. (c) Bhattacharya, S.; Xiong, Z.; Wu, G.; Chen, P.; Feng, Y. P.; Majumder, C.; Das, G. P. *J. Phys. Chem. C* **2012**, *116*, 8859.

(26) (a) Chua, Y. S.; Wu, H.; Zhou, W.; Udovic, T. J.; Wu, G.; Xiong, Z.; Wong, M. W.; Chen, P. *Inorg. Chem.* **2012**, *51*, 1599. (b) Chua, Y.

S.; Wu, G.; Xiong, Z.; Karkamkar, A.; Guo, J.; Jian, M.; Wong, M. W.; Autrey, T.; Chen, P. *Chem. Commun.* **2010**, *46*, 5752.
(27) Shimoda, K.; Doi, K.; Nakagawa, T.; Zhan, Y.; Miyaoka, H.; Ichikawa, T.; Tansho, M.; Shimizu, T.; Burrell, A. K.; Kojima, Y. *J. Phys. Chem. C* **2012**, *116*, 5957.
(28) (a) Kim, D. Y.; Singh, N. J.; Lee, H. M.; Kim, K. S. *Chem.—Eur. J.* **2009**, *15*, 5598. (b) Wang, K.; Zhang, J. G.; Yang, W.; Wu, M.; Man, T. T.; Zhang, T. L.; Zhang, S. W. *Struct. Chem.* **2013**, *24*, 1527. (c) Dong Young, K.; Han Myoung, L.; Jongcheol, S.; Seung Koo, S.; Kim, K. S. *Phys. Chem. Chem. Phys.* **2010**, *12*. (d) Wu, C.; Wu, G.; Xiong, Z.; David, W. I. F.; Ryan, K. R.; Jones, M. O.; Edwards, P. P.; Chu, H.; Chen, P. *Inorg. Chem.* **2010**, *49*, 4319. (e) Shevlin, S. A.; Kerkeni, B.; Guo, Z. X. *Phys. Chem. Chem. Phys.* **2011**, *13*, 7649.

dx.doi.org/10.1021/ic500679b | *Inorg. Chem.* 2014, 53, 7334−7339